

Article

Time-Dependent Behavior of Waste Lithium-Ion Batteries in Secondary Copper Smelting

Anna Klemettinen ^{1,*} , Lassi Klemettinen ¹ , Radosław Michallik ², Hugh O'Brien ² and Ari Jokilaakso ¹ 

¹ Department of Chemical and Metallurgical Engineering, School of Chemical Engineering, Aalto University, Kemistintie 1, P.O. Box 16100, 00076 Aalto, Finland

² Geological Survey of Finland, Vuorimiehentie 2, 02150 Espoo, Finland

* Correspondence: anna.klemettinen@aalto.fi

Abstract: As the electrification sector expands rapidly, the demand for metals used in batteries is increasing significantly. New approaches for lithium-ion battery (LIB) recycling have to be investigated and new technologies developed in order to secure the future supply of battery metals (i.e., lithium, cobalt, nickel). In this work, the possibility of integrating LIB recycling with secondary copper smelting was further investigated. The time-dependent behavior of battery metals (Li, Co, Ni, Mn) in simulated secondary copper smelting conditions was investigated for the first time. In the study, copper alloy was used as a medium for collecting valuable metals and the distribution coefficients of these metals between copper alloy and slag were used for evaluating the recycling efficiencies. The determined distribution coefficients follow the order Ni >> Co >> Mn > Li throughout the time range investigated. In our study, the evolution of phases and their chemical composition were investigated in laboratory-scale experiments under reducing conditions of oxygen partial pressure $p(\text{O}_2) = 10^{-10}$ atm, at 1300 °C. The results showed that already after 1 h holding time, the major elements were in equilibrium. However, based on the microstructural observations and trace elements distributions, the required full equilibration time for the system was determined to be 16 h.

Keywords: recycling; circular economy; kinetics; pyrometallurgy



Citation: Klemettinen, A.; Klemettinen, L.; Michallik, R.; O'Brien, H.; Jokilaakso, A. Time-Dependent Behavior of Waste Lithium-Ion Batteries in Secondary Copper Smelting. *Batteries* **2022**, *8*, 190. <https://doi.org/10.3390/batteries8100190>

Academic Editor: Joeri Van Mierlo

Received: 31 August 2022

Accepted: 13 October 2022

Published: 17 October 2022

Publisher's Note: MDPI stays neutral with regard to jurisdictional claims in published maps and institutional affiliations.



Copyright: © 2022 by the authors. Licensee MDPI, Basel, Switzerland. This article is an open access article distributed under the terms and conditions of the Creative Commons Attribution (CC BY) license (<https://creativecommons.org/licenses/by/4.0/>).

1. Introduction

It is evident that the demand for lithium-ion batteries (LIBs) is significantly increasing as the electrification sector expands. According to the International Energy Agency (IEA), roughly 15–25 million electric vehicles will be sold annually by 2025 and 25–40 million by 2030 [1]. As the production of rechargeable batteries increases, the demand for battery raw materials rises as well. The energy transformation is the main factor influencing the global demand for lithium, cobalt and nickel [2]. As most of the battery metals are produced only in a few countries, supply risks, as well as environmental and ethical issues, may occur [3].

One of the important strategies for circulating the critical battery materials in the supply chain is finding the most efficient ways for recovering the materials from waste LIBs [4]. In recent years, great effort has been made globally to develop efficient recycling technologies for lithium-ion batteries, and these technologies have been described in several review papers [4–9].

Currently, pyrometallurgical processes are widely used in industry as a route for recycling various metal-rich waste streams, including batteries. The advantages and disadvantages of high-temperature processes in recycling were described in the work of Chen et al. [10]. The authors highlighted that the pyrometallurgical treatment process is simple and mature, and does not require physical pretreatment (e.g. sorting or size reduction) [10]. Moreover, pyrometallurgical processes have the advantage of high-rate chemical reactions, which lead to high treatment capacities [7]. Pyrometallurgical methods for battery recycling include thermal pretreatment, roasting/calcination and smelting.

Smelting is an effective pyrometallurgical process in which battery scrap is heated above its melting point to achieve the separation of metals in liquid phases through the reduction and formation of a metal alloy [7]. The metal alloy formed in the system acts as a medium to recover some of the battery metals, such as cobalt, copper and nickel, which are typically the more expensive ones. Other metals like lithium, aluminum and manganese end up in the slag [10,11], where it may currently be unfeasible to recover them. Some of the possible smelting processes designed for the recycling of LiBs were described in the review paper of Makuza et al. [7]. Another possible option is to use existing primary and secondary copper smelters, which allows for eliminating the capital costs of building a new recycling facility. A variety of copper smelting processes can be integrated not only with the recycling of battery metals but also for the recovery of other valuable metals from the waste electric and electronic equipment (WEEE) [12]. However, the integration of copper smelting processes with the recycling of batteries and/or WEEE brings many new elements to the process circuits and changes the concentrations of existing elements. According to Jak [13] the demand for reliable data on phase equilibria, thermodynamic and physical properties in metallurgical and recycling industries is increasing due to the growing economical competition, more strict environmental regulations, and availability of more advanced methods used in process control. Therefore, the behavior of different elements under different smelting conditions must be studied in order to understand the phenomena and optimize the processes. However, to optimize smelting processes and to obtain high recoveries of valuable metals, not only thermodynamic data is needed but also the kinetic behavior of trace elements and their reaction mechanisms occurring during the processes need to be known [14].

Several studies have been conducted obtaining thermodynamic data on how elements typical for WEEE behave in simulated processes of primary and secondary copper smelting in equilibrium conditions [15–27]. In our previous studies [11,28], the behavior of battery metals (Li, La, Co, Cu, Mn and Ni) was investigated in equilibrium in reducing conditions (between 10^{-11} and 10^{-8} atm oxygen partial pressure) at 1300 °C. In those studies, the influence of MgO content on slag chemistry and trace element distribution was investigated.

However, the time-dependent behavior of battery metals in copper smelting has not been studied before. The first data on the kinetic behavior of trace elements in copper flash smelting were provided by Wan et al. [14,28–31]. In these studies, the time-dependent behavior of precious metals Au, Ag, Pt, Pd as well as impurity elements As, Sb and Bi during copper flash smelting was investigated experimentally. The time-dependent behavior of Rare Earth Elements (REEs) in copper matte-slag systems in primary copper smelting conditions was researched experimentally by Klemettinen et al. [32].

The main goal of this study was to investigate how fast the battery metals (cobalt, lithium, nickel, manganese) distribute between different phases in laboratory-scale experiments simulating secondary copper smelting conditions. The evolution of different phases in the system as a function of time was investigated under reducing conditions at high temperatures. In comparison to previous studies [11,28] where the battery metals were added to the system as pure substances, industrial battery scrap was used in the current study.

The achievement of equilibrium is obviously the most important and common uncertainty in thermodynamic phase equilibria investigations [13]. In previous equilibrium studies by us and other researchers, the attainment of equilibrium has been confirmed by conducting experiments for different times and analyzing the composition as well as homogeneity of obtained phases. However, the required equilibration time has been determined only based on major element composition. In this work, the aim was to investigate the time required for the trace and ultra-trace elements to reach equilibrium distributions between copper alloy and slag. Electron probe microanalysis (EPMA) and laser ablation-inductively coupled plasma-mass spectrometry (LA-ICP-MS) analysis techniques were utilized for phase composition quantifications after high-temperature holding and rapid quenching.

2. Experimental

2.1. Materials

The initial sample mixture was comprised of synthetic slag and copper alloy mixtures as well as industrial battery scrap. The mixture of slag contained 15 wt% Al₂O₃ (powder, Sigma Aldrich, St. Louis, MO, USA), 51 wt% Fe₂O₃ (powder, Alfa Aesar, Kandel, Germany), 28 wt% SiO₂ (powder, 40 mesh, Alfa Aesar, Kandel, Germany) and 6% MgO (powder, 325 mesh, Alfa Aesar, Kandel, Germany). The initial Fe/SiO₂ mass ratio was 1.3. All components were mixed in a mortar to obtain a fine and homogenous mixture.

The copper alloy was a mixture of pure metal powders: 93 wt% Cu (powder, Alfa Aesar, Kandel, Germany), 5 wt% Sn (powder, 100 mesh, Alfa Aesar, Kandel, Germany) and 2 wt% Ni (powder, APS 3-7 micron, Alfa Aesar, Kandel, Germany).

The battery scrap was obtained from a Finnish industrial operator. The used fraction was fine cathode material with a high concentration of Co. The chemical composition of the battery scrap was analyzed using four acid digestion of a sample followed by multielement analysis with ICP-OES. Additionally, the carbon content was analyzed with combustion analysis with a Leco analyzer. All analyses were done by CRS Laboratories Oy (Outokumpu, Finland) and the results are summarized in Table 1.

Table 1. Chemical composition of industrial battery scrap used in the experiments. The remainder is oxygen.

Element Concentration/wt%													
Al	Ca	Co	Cu	Fe	K	Li	Mg	Mn	Na	Ni	P	Zn	C
1.60	0.03	26.5	2.70	0.61	0.05	3.87	0.09	1.67	0.06	2.74	0.45	0.04	33.0

In every experiment, the starting mass of the battery scrap was approximately 4 wt% of the mass of the copper alloy. The amount of battery scrap was chosen so that the initial concentration of Co in the sample was 1 wt% of the mass of copper alloy, as in our previous equilibrium study [11].

2.2. Experimental Methods

The applied experimental method was based on heating the sample charge at a controlled temperature and gas atmosphere followed by rapid quenching into the ice-water mixture. Experiments were conducted under simulated black copper smelting conditions at 1300 °C at reducing conditions of oxygen partial pressure $p_{O_2} = 10^{-10}$ atm. The laboratory vertical furnace (Nabertherm, Lilienthal, Germany, RHTV 120-150/18) with MoSi₂ heating elements and an alumina reaction tube (Frialit AL 23; Friatec AG, Mannheim, Germany; 45 mm OD and 38 mm ID). A calibrated S-type Pt/Pt10Rh thermocouple (Johnson-Matthey, London, UK) with an uncertainty of ± 3 °C was used to control the experimental temperature. The furnace setup was presented in detail in a previous study of Klemettinen et al. [22].

The prepared mixture containing slag, copper alloy and battery scrap was placed in an alumina crucible held by a Pt-wire basket. The first 0.2 g of the metal alloy was weighed into the crucible, then approximately 0.008 g of battery scrap was added on top of the metal alloy, followed by adding 0.2 g of slag on top of the mixture. The weight ratio between metal alloy, slag and battery scrap was 1:1:0.04. The crucible was hooked with a platinum-rhodium wire and pulled up to the hot zone of the furnace. More details regarding the procedure of introducing the sample into the furnace were described in a previous study of Dańczak et al. [28]. The samples were kept in the hot zone for different times, from 1.5 min to 48 h. Holding times of less than 1.5 min were tested but omitted since the samples did not melt completely. The gas atmosphere was obtained by mixing CO and CO₂ with flow rates of 174.5 mL/min and 125.6 mL/min, respectively. The gas flow rates were calculated using MTDATA software and the SGTE pure substances database [33]. During experiments, the gas flow gates were controlled using mass flow controllers (DFC 26, Aalborg, Orangeburg, NY, USA). After appropriate contact times, the samples were rapidly quenched in an ice-

water mixture without compromising the gas atmosphere. The quenched samples were cut in half, mounted in epoxy resin, ground, polished and carbon coated (Figure 1).



Figure 1. Photograph of a typical sample cross-section in epoxy after analyses. The violet color of the copper alloy is a result of carbon coating. The small holes on the slag and copper alloy are laser pits produced by LA-ICP-MS. Photo: Aalto University, Eren Öztekin.

2.3. Sample Analysis

The sample microstructures were analyzed with SEM (Scanning Electron Microscope; Mira3, Tescan, Czech Republic) and the composition of phases was preliminarily investigated with EDS (Energy Dispersive Spectrometer, Thermo Fisher Scientific, Waltham, MA, USA). For more accurate phase composition analyses regarding major and trace elements, EPMA and LA-ICP-MS were used, respectively.

The EPMA analyses were obtained with CAMECA SX100 electron microprobe at the Geological Survey of Finland (GTK) using WDS (wavelength-dispersive spectrometry) technique. The accelerating voltage and beam current were 20 kV and 60 nA, respectively. A focused beam was used for the spinel phase, while a defocused beam was used for slag (20 μm) and the metal phase (50 μm). Analytical results were corrected using the PAP on-line correction program [34]. Natural minerals and synthetic metals were used as standards as follows: obsidian for O ($K\alpha$), quartz for Si ($K\alpha$), almandine for Al ($K\alpha$), diopside for Mg ($L\beta$), hematite for Fe ($M\alpha$), rhodonite for Mn ($K\alpha$), cobaltite for Co ($K\alpha$), copper for Cu ($L\alpha$), tin for Sn ($L\alpha$) and nickel for Ni ($K\alpha$).

The concentrations of several elements fell under the detection limits of EPMA, so their concentrations were quantified using LA-ICP-MS at GTK. The details of the equipment used have been presented previously [11]. The metal alloy was analyzed using a 50 μm diameter laser spot size, 10 Hz pulse frequency and 3.2 J/cm² power. External calibration was conducted using UQAC FeS-1 pressed sulfide pellet [35] and USGS MASS1 [36] was used as a monitor. ⁶⁰Ni isotope was used as the internal standard. The slag was also analyzed using 50 μm diameter spots, but with 5 Hz pulse frequency and 2.17 J/cm² power. NIST 610 and 612 [37] were used for calibration and as a monitor, respectively. The internal standard was the ²⁹Si isotope.

The analysis protocol followed a 2-s pause, 5 pre-ablation shots, 20-s flushing, 20-s background analysis and either 300 (metal, 10 Hz) or 200 (slag, 5 Hz) laser shots. The mass signal intensities were converted to elemental concentrations using Glitter software [38].

The detection limits obtained using EPMA and LA-ICP-MS are shown in Table S1 in Supplementary Materials.

3. Results

3.1. Time-Dependent Evolution of Sample Microstructure

Figure 2 shows the general microstructure of a sample after a short (10 min), and long (48 h) holding time. Every sample consisted of a glassy slag phase, metal alloy, alumina crucible and primary spinel phase. In every sample, the spinel grains, so-called discrete spinels, were found within the slag. Additionally, in all samples, a spinel layer was formed between the slag and alumina crucible. However, the thickness and uniformity of this layer increased significantly as the holding time increased. The holding time did not seem to influence the microstructure of the metal alloy, as a large alloy droplet was observed in every sample, even after 1.5 min time. No quantifiable differences were found between the visual appearance of metal alloys in samples after different holding times.

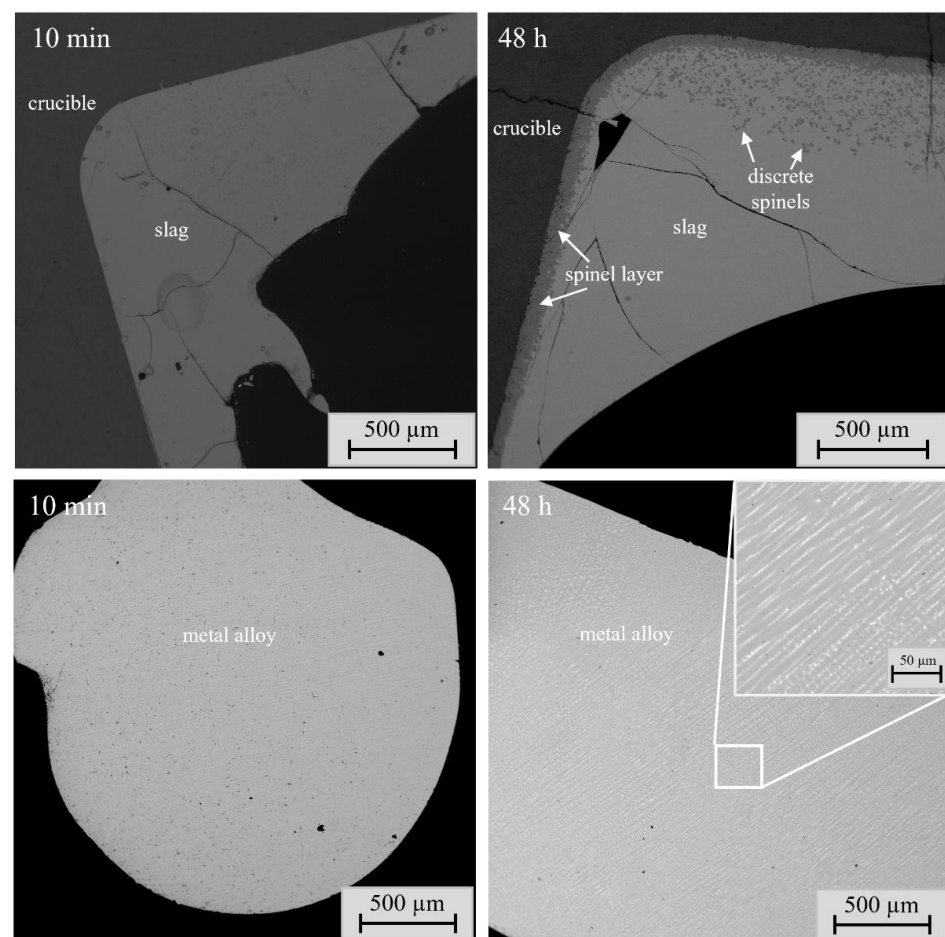


Figure 2. General microstructure of a sample after 10 min (left side) and 48 h (right side) holding time.

The visual evolution of discrete spinels as a function of increasing holding time is presented in Figure 3. In the samples after short holding times (1.5–5 min), the discrete spinel grains were smaller than 10 microns and seemed to be ‘dispersed’ within the whole slag phase. Moreover, these spinels did not have a well-defined shape or size. With longer holding times, the individual spinel grains seemed to accumulate and increase in size, which can be seen in the microstructure image of the sample after 10 min holding time. However, these grains were still not big enough to be properly analyzed with the EPMA technique, without obtaining a signal from the surrounding slag phase. The size

of the spinel grains was enough for the compositional analysis with EPMA after 30 min holding time. As the holding time increased further, the spinel grains grew in size and had more defined shapes. The color of the spinel in the SEM-backscattered electron images also became darker, corresponding to the change in composition from iron-oxide-rich to alumina-rich [24]. There were no visible differences in the sample microstructures after 16 h contact time.

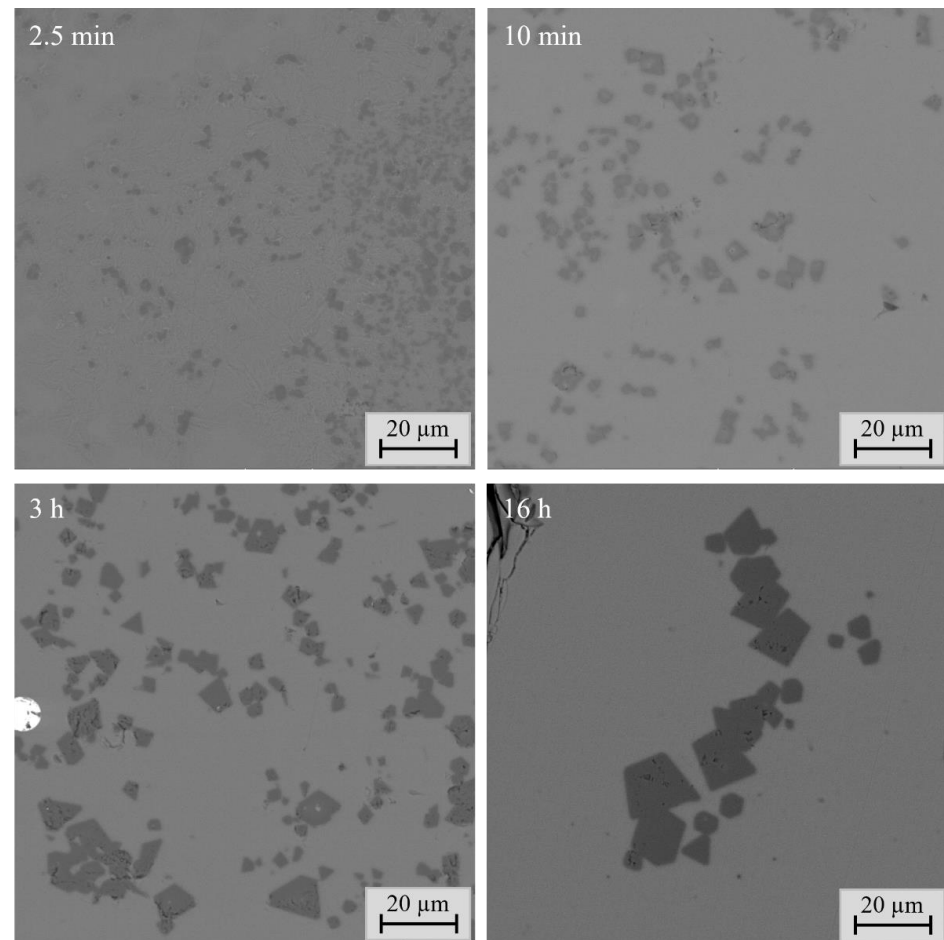


Figure 3. Microstructures of the slag and discrete spinels formed in samples at different holding times. The change of the spinel crystals from light gray to darker gray illustrates the compositional change from iron oxide-rich to alumina-rich as the contact time is prolonged.

3.2. Concentration of Major Elements in Slag and Spinel

The concentrations of major elements (Fe, Al, O, Mg and Si) were analyzed with the EPMA technique. Figure 4 shows these concentrations in slag and spinel as a function of time. The biggest changes in the concentrations of major elements in slag occurred within the first 5 min.

The concentration of Fe in slag first decreased from 36.5 wt% at 1.5 min holding time to 34.4 wt% after 2.5 min holding time, and as the time increased to 20 min, the concentration increased to 38.4 wt%. After 48 h, the Fe concentration was 35.4 wt%. Oxygen concentration in slag firstly also decreased slightly, and the final value after 48 h was 38.9 wt%. The concentration of Al in the slag increased from 6.4 wt% after 1.5 min to 7.9 wt% after 48 h, whereas the concentration of Mg decreased slightly from 3.4 wt% to 3.1 wt% within the same time. The concentration of Si in the slag remained relatively constant throughout the time series, with the final value being 15.5 wt% after 48 h.

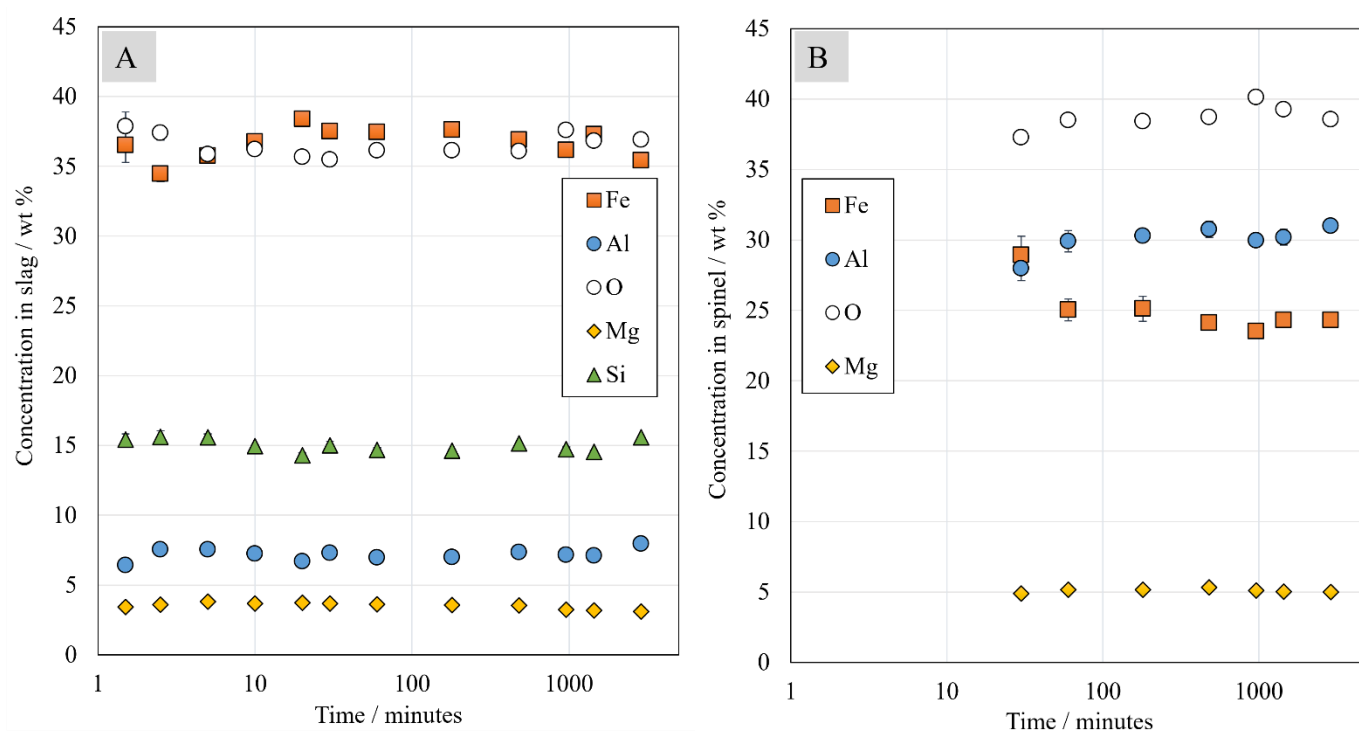


Figure 4. Concentrations of major elements in the slag (A) and spinel (B) phase as a function of time.

The spinel composition was analyzed only in the samples with holding times of 30 min or longer, as the discrete spinels formed after shorter times were not big enough to be reliably analyzed with EPMA. The concentration of Fe in spinel decreased from 28.9 wt% to 24.3 wt% as the contact time increased from 30 min to 48 h, whereas the concentrations of Al and O increased from 27.9 wt% to 31.0 wt% and from 37.3 wt% to 38.5 wt%, respectively, within the same time. After 60 min holding time, the concentrations of Fe, O and Al in the spinel remained relatively constant. The concentration of Mg was the same, approximately 5 wt%, regardless of the holding time. Additionally, the spinel grains contained small amounts of Si, the concentration of which varied between 0.1 and 0.5 wt%. It should be mentioned that there were large deviations in the analyzed Si concentrations in spinel in each sample. The spinel grains also contained low concentrations of Co and Ni. After 30 min holding time, cobalt concentration was approximately 0.4 wt% and it increased to 0.8 wt% after 48 h holding time. The concentration of Ni in spinel varied randomly between 0.05 and 0.1 wt%. The concentrations of all elements in the slag and spinel are presented in Tables S2–S5 in Supplementary Materials.

3.3. Composition of Metal Alloy

The concentrations of Cu, Co, Ni, O and Sn in the metal alloy, analyzed with EPMA, are presented in Figure 5. The metal alloy was formed already after 1.5 min holding time and the Cu concentration at that time was 94.3 wt%. With the increasing holding time, Cu concentration varied between 93 and 96 wt%, with the final value being 94.1 wt% after 48 h. The concentration of Sn in the metal alloy reached 3.5 wt% after the shortest time of 1.5 min. With longer holding times, its concentration varied significantly between 1.7 and 4.2 wt%. However, the concentration of Sn after the longest holding time of 48 h was 3.4 wt%; similar as after 1.5 min. The large variation in Sn concentration can be attributed to the stripe-like structure of the metal alloy shown in Figure 2, bottom right corner. Some Sn evaporation may also have taken place [23], contributing to the large concentration variations between samples as well as within one sample.

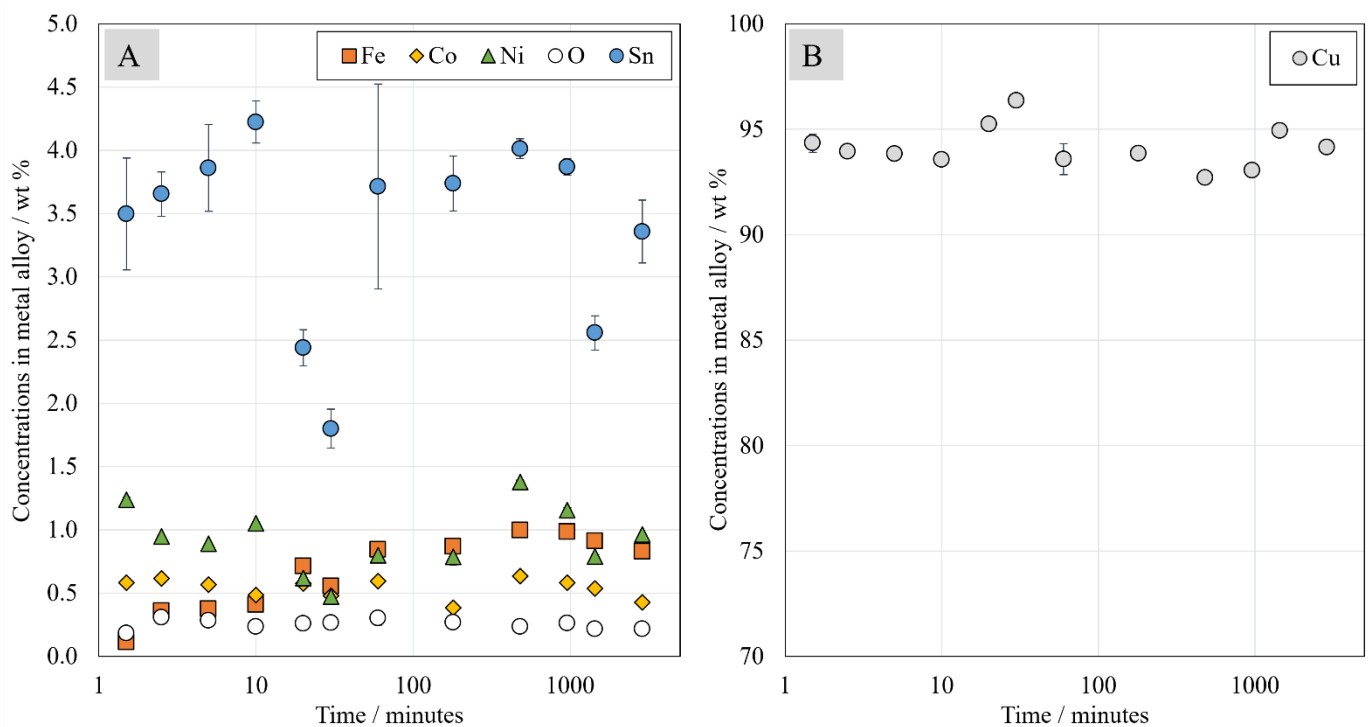


Figure 5. Concentrations of major elements (A) Fe, Co, Ni, O, Sn and (B) Cu in metal alloy.

The concentration of iron in the metal alloy increased from 0.1 wt% after 1.5 min to 1 wt% after 8 h holding time. After this time, its concentration decreased slightly to 0.8 wt%. The concentration values of nickel were found to be scattered between 0.5 and 1.4 wt% at different holding times, which can also be attributed to the stripe-like structure of the alloy, i.e., the brighter stripes (Figure 2) contain higher concentrations of nickel and tin than the matrix. Generally, when tin and nickel concentrations in the alloy decreased, copper concentration increased. The cobalt and oxygen concentrations in the alloy remained quite stable as a function of time, approximately 0.5 wt% and 0.2 wt%, respectively. It should be highlighted that after 1 h holding time, the concentrations of Co, Cu, Ni, Fe and O reached the same values as after 48 h.

4. Discussion

In a multi-element system, the change in concentration of elements in the slag or metal alloy may not always represent the actual change in the recovery of these metals to the metal phase. In our study, the industrial battery scrap used in the experiments was a heterogeneous mixture of chemical compounds. Therefore, the starting concentrations of metals in the system may slightly vary in each experiment. When evaluating the recovery of different (trace) metals to the alloy phase, the distribution coefficients of these metals between alloy and slag provide information independent of the slight variations in the starting concentration between different samples.

In metal–slag equilibria at a high temperature, the oxidic dissolution reaction of a minor element X with a valence of $2v$ in the slag can be expressed by Equation (1).



The equilibrium constant K for the above reaction can be described by the activities of X in metal and XO_v in slag, according to Equation (2)

$$K = \frac{a_{XO_v}}{a_X \cdot p_{O_2}^{v/2}} \quad (2)$$

where a_i is the activity of a chemical species and p_{O_2} is oxygen partial pressure.

As described in the work of Takeda and Yazawa [39,40], the distribution ratio of an element X between molten metal and the slag is expressed in Equation (3):

$$L^{Cu/s}(X) = \frac{[X \text{ wt}\%]}{(X \text{ wt}\%)} = \frac{[n_T] \cdot (\gamma_{XO_v})}{K \cdot (n_T) \cdot [\gamma_X] \cdot p_{O_2}^{v/2}} \quad (3)$$

where the [] and () brackets represent the copper alloy and slag phases, respectively. In the above equation, $L^{Cu/s}(X)$ is the distribution coefficient of element X between copper alloy and slag; n_T is the total moles of constituents in 100 g of each phase and γ is the activity coefficient.

The distribution coefficient described with Equation (3) is often used while studying the behavior of trace metals in different systems in metallurgical processes. In this study, copper alloy is used as a medium for collecting the trace metals and the distribution coefficients between copper alloy and slag are essential parameters utilized for evaluating the recycling efficiencies of different metals in copper smelting. If the distribution coefficient of a metal is below 1 (or 0 in logarithmic scale), most of this metal distributes into the slag phase, where its recovery is difficult.

The distribution coefficients of metals are typically determined at equilibrium conditions and presented as a function of oxygen partial pressure or temperature, or of concentration of additives (e.g., CaO, MgO, K₂O). In this study, the experiments were conducted at a constant temperature and oxygen partial pressure. In all experiments, the starting composition of the mixture was also constant, neglecting the possible variations in battery scrap composition mentioned earlier. The only controlled variable was the high-temperature holding time. Therefore, in this study, the distribution coefficients of different metals were presented as a function of contact time (t). The distribution coefficient values of metals determined at selected times (t) can be described by Equation (4) [14].

$$L^{Cu/s}(X)_t = [X \text{ wt}\%]_t / (X \text{ wt}\%)_t \quad (4)$$

Figure 6 shows the logarithms of distribution coefficients of Li, Mn, Ni, Sn, Co, Pb, Fe and Cu between copper alloy and the slag as a function of holding time. Comparisons with our previous equilibrium studies [11,28] are also presented. The calculated values of distribution coefficients and their uncertainties are presented in Table S6 in Supplementary Materials.

For copper and iron, the most significant changes in the calculated distribution coefficients occurred before 2.5 min of holding. During that time, the logarithmic distribution coefficient of copper decreased from 3.0 at 1.5 min to 2.2 at 2.5 min and the logarithmic distribution coefficient of iron increased from -2.5 to -2.0 . After 2.5 min holding time, the distribution coefficient of copper remained stable, at approximately 2.2 in log scale, all the way up to the longest time. In comparison, the logarithmic distribution coefficient of iron increased further up to -1.6 during the first 60 min. After that, its value remained stable. The low value of iron distribution coefficient indicates that most of the iron remained in the slag phase as iron oxides.

Similar to copper and iron, the distribution coefficient of cobalt decreased the most significantly before 2.5 min holding time, from 1.0 to 0.0 in a log scale. After that time, it increased slightly to 0.1. This is in agreement with the results of our previous equilibrium study [11]. The logarithmic distribution coefficient value close to 0 indicates that cobalt is basically evenly distributed between copper alloy and the slag at $p_{O_2} = 10^{-10}$ atm.

In the case of lead, its calculated logarithmic distribution coefficient changed between 1.0 and 1.5 at different contact times without a visible trend. The concentration of lead in the slag decreased close to or even below the LA-ICP-MS detection limits at 8 h and longer holding times, which contributes to the uncertainty of the true distribution coefficient values after long holding times.

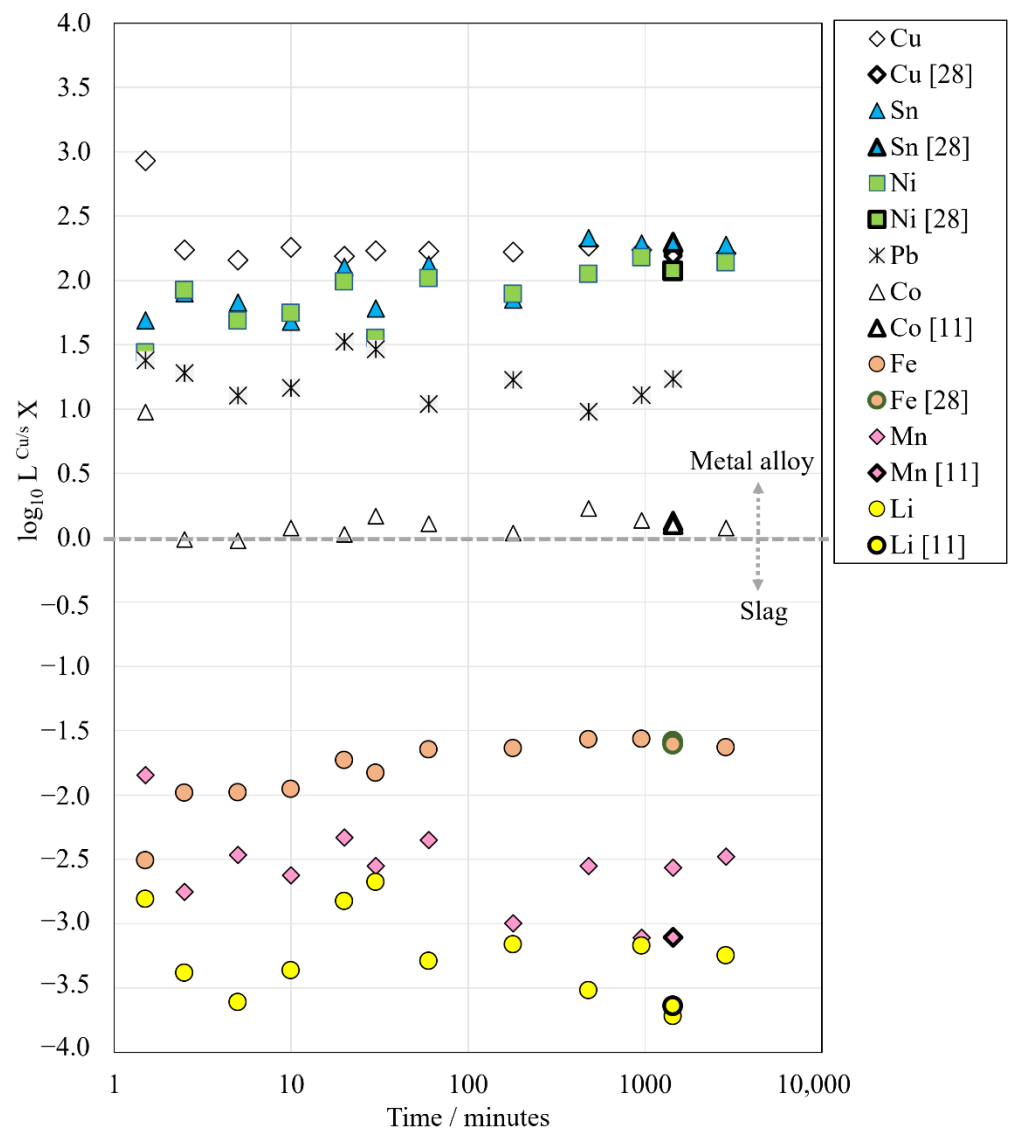


Figure 6. The distribution coefficients of Li, Mn, Fe, Co, Pb, Ni, Sn and Cu between copper alloy and molten slag as a function of holding time.

The distribution coefficients of nickel and tin increased as the holding time increased, from 1.4 to 2.1 and from 1.7 to 2.3 in the log scale, respectively. After 16 h holding time, nickel and tin distribution coefficient values remained relatively stable.

The logarithmic distribution coefficients of lithium and manganese have very negative values and are much lower in comparison to the other trace elements in this study, which shows that lithium and manganese deport strongly into the slag phase rather than into copper alloy under the investigated conditions. Their distribution coefficient values seem to be fluctuating without clear trends, which can be explained by their extremely low concentrations in the copper alloy. However, the values are in fair agreement with our previous equilibrium study [11].

The calculated distribution coefficients $L^{Cu/s}(X)_t$ of battery metals (Li, Co, Ni, Mn) followed the order of $Ni \gg Co \gg Mn > Li$ at both the shortest (1.5 min) and the longest (48 h) holding time. This order corresponds to the Ellingham diagram showing the stabilities of battery metal oxides [11].

5. Conclusions

As battery metals such as lithium, cobalt and nickel, are characterized by high demand and/or supply risks, new ways for securing their availability in the future have to be developed. Recycling lithium-ion batteries through high-temperature processes is a viable option for recovering some of the valuable metals within. Integration of battery recycling with already existing pyrometallurgical operations helps decrease investment costs compared to building greenfield facilities. However, changing the feeds of existing smelters introduces many new elements into the system, and therefore influences the process chemistry and recovery of valuables.

In this study, the possibility of integrating LIB recycling with secondary copper smelting was further investigated. The behavior of battery metals in simulated reducing conditions of secondary copper smelting was investigated as a function of time for the first time. The evolution of phases in the system and the required equilibration time were investigated as well.

The visual observations regarding sample microstructure are important for determining the equilibration time. One important criterion for the achievement of equilibrium is that the phases present do not change as a function of equilibration time [23]. In our study, already after 1.5 min holding time all equilibrium phases, i.e., slag, metal alloy and spinel were present and remained in the samples with the longer holding times. Other important criteria are that all phases are homogeneous, and the microstructure does not change as a function of time [13,23]. In this study, the most significant change in sample microstructure was connected to the spinel layer and spinel grains. The spinel layer between the slag and crucible became much thicker and more uniform as a function of time, and the size of the discrete spinels increased as well. These changes were observed until 16 h holding time. After 16 h, the phases were homogeneous and the microstructures of samples did not change anymore.

In this study, the chemical compositions were analyzed using the state-of-the-art direct phase analysis methods EPMA and LA-ICP-MS. The concentrations of major elements in the slag remained surprisingly constant throughout the investigated time series, apart from iron, which also stabilized at approximately 30 min holding time. In spinel, the concentrations of major elements changed until 1 h holding time, after which they remained basically stable over the remaining time. The concentrations of major elements in the metal alloy after 1 h holding time reached very similar values as after 48 h contact time.

The results indicated that already after 1 h holding time, the major elements are in equilibrium. However, the observations regarding sample microstructure as well as trace element distribution coefficients suggest that a 16 h holding time is required to obtain steady-state microstructure and homogeneous phases. Therefore, the equilibration time cannot be verified only based on the concentrations of major elements. The distribution of trace elements between metal alloy and slag, as well as microstructural observations, must be taken into consideration. Based on the data presented in Figure 6 as well as the microstructural observations, it can be concluded that 16 h is sufficient for equilibrating the samples of this study, which also verifies that the equilibration times chosen in our previous studies have been sufficient [11,20,22,24,28]. The distribution coefficients of Pb, Li and Mn were somewhat fluctuating even after 16 h due to analysis difficulties associated with extremely low concentrations in slag (Pb) or alloy phase (Li, Mn).

The distribution coefficients of battery metals (Li, Co, Ni, Mn) between metal alloy and slag were investigated as a function of time and their values followed the order of $Ni \gg Co \gg Mn > Li$ at both the shortest (1.5 min) and the longest (48 h) holding time. The logarithmic values of the distribution coefficients suggest that most of the Ni can be recovered to the metal phase. In the case of cobalt, half of it can be recovered in the metal alloy and the other half is deported to the slag under the experimental conditions applied in this study. Lithium and manganese heavily deport to the slag phase and are basically lost in current copper smelting operations.

Supplementary Materials: The following supporting information can be downloaded at: <https://www.mdpi.com/article/10.3390/batteries8100190/s1>. Table S1: EPMA and LA-ICP-MS detection limits (in ppm). Table S2: Average concentrations and standard deviations of aluminum, iron, magnesium, oxygen, silicon and copper in metal alloy, slag and spinel. All results from EPMA. Table S3: Average concentrations and standard deviations of cobalt, nickel and tin in metal alloy, slag and spinel. All results from EPMA. Table S4: Average concentrations and standard deviations of Li, Co, Mn, and Ni in metal and slag phases, based on LA-ICP-MS analyses. Table S5: Average concentrations and standard deviations of Cu, Pb and Sn in metal and slag phases, based on LA-ICP-MS analyses. Table S6: Distribution coefficients of Cu, Sn, Ni, Pb, Co, Fe, Mn and Li between metal alloy and slag and their uncertainties.

Author Contributions: Conceptualization, L.K. and A.J.; methodology, A.K., L.K., R.M., H.O. and A.J.; software, L.K., R.M. and H.O.; validation, A.K., L.K. and R.M.; formal analysis, A.K., L.K. and R.M.; investigation, A.K. and L.K.; resources, R.M., H.O. and A.J.; data curation, A.K., L.K. and R.M.; writing—original draft preparation, A.K. and L.K.; writing—review and editing, R.M., H.O. and A.J.; visualization, A.K. and L.K.; supervision, A.J.; project administration, A.J.; funding acquisition, A.J. All authors have read and agreed to the published version of the manuscript.

Funding: This work was conducted in the Business Finland-funded SYMMET project (project no 3891/31/2018). Financial support was also received from the Academy of Finland-funded GoverMat project (Decision No. 346728).

Data Availability Statement: All data is available in the Supplementary Materials.

Acknowledgments: The experimental work was conducted in the Business Finland funded SYMMET project (project no 3891/31/2018). The Academy of Finland's RAMI infrastructure, based jointly at Aalto University, GTK Espoo and VTT Espoo, was utilized in this work.

Conflicts of Interest: The authors declare no conflict of interest.

References

1. IEA. *Entering the Decade of Electric Drive? Technology Report, Global EV Outlook*; International Energy Agency: Paris, France, 2020; 276p.
2. Tuomela, P.; Törmänen, T.; Michaux, S. *Strategic Roadmap for the Development of Finnish Battery Mineral Resources*; Technical Report; Geological Survey of Finland: Espoo, Finland, 2021. [[CrossRef](#)]
3. Dehaine, Q.; Michaux, S.P.; Pokki, J.; Kivinen, M.; Butcher, A.R. Battery minerals from Finland: Improving the supply chain for the EU battery industry using a geometallurgical approach. *Eur. Geol. J.* **2020**, *49*, 5–11. [[CrossRef](#)]
4. Islam, M.T.; Iyer-Raniga, U. Lithium-Ion Battery Recycling in the Circular Economy: A Review. *Recycling* **2022**, *7*, 33. [[CrossRef](#)]
5. Velázquez-Martínez, O.; Valio, J.; Santasalo-Aarnio, A.; Reuter, M.; Serna-Guerrero, R. A Critical Review of Lithium-Ion Battery Recycling Processes from a Circular Economy Perspective. *Batteries* **2019**, *5*, 68. [[CrossRef](#)]
6. Sommerville, R.; Shaw-Stewart, J.; Goodship, V.; Rowson, N.; Kendrick, E. A review of physical processes used in the safe recycling of lithium ion batteries. *Sustain. Mater. Technol.* **2020**, *25*, e00197. [[CrossRef](#)]
7. Makuza, B.; Tian, Q.; Guo, X.; Chattopadhyay, K.; Yu, D. Pyrometallurgical options for recycling spent lithium-ion batteries: A comprehensive review. *J. Power Sources* **2021**, *491*, 229622. [[CrossRef](#)]
8. Piątek, J.; Afyon, S.; Budnyak, T.M.; Budnyk, S.; Sipponen, M.H.; Slabon, A. Sustainable Li-Ion Batteries: Chemistry and Recycling. *Adv. Energy Mater.* **2021**, *11*, 2003456. [[CrossRef](#)]
9. Neumann, J.; Petranikova, M.; Meeus, M.; Gamarra, J.D.; Younesi, R.; Winter, M.; Nowak, S. Recycling of Lithium-Ion Batteries—Current State of the Art, Circular Economy, and Next Generation Recycling. *Adv. Energy Mater.* **2022**, *12*, 2102917. [[CrossRef](#)]
10. Chen, M.; Ma, X.; Chen, B.; Arsenault, R.; Karlson, P.; Simon, N.; Wang, Y. Recycling End-of-Life Electric Vehicle Lithium-Ion Batteries. *Joule* **2019**, *3*, 2622–2646. [[CrossRef](#)]
11. Dańczak, A.; Klemettinen, L.; Kurhila, M.; Taskinen, P.; Lindberg, D.; Jokilaakso, A. Behavior of Battery Metals Lithium, Cobalt, Manganese and Lanthanum in Black Copper Smelting. *Batteries* **2020**, *6*, 16. [[CrossRef](#)]
12. Forsén, O.; Aromaa, J.; Lundström, M. Primary Copper Smelter and Refinery as a Recycling Plant—A System Integrated Approach to Estimate Secondary Raw Material Tolerance. *Recycling* **2017**, *2*, 19. [[CrossRef](#)]
13. Jak, E. Integrated experimental and thermodynamic modelling research methodology for metallurgical slags with examples in the copper production field. In Proceedings of the Ninth International Conference on Molten Slags, Fluxes and Salts, Beijing, China, 27–31 May 2012. Available online: <https://www.pyrometallurgy.co.za/MoltenSlags2012/W077.pdf> (accessed on 9 August 2022).
14. Wan, X. Experimental Investigation on Time-Dependent Recycling Behaviour of WPCBs in Copper Flash Smelting Conditions. Ph.D. Thesis, Aalto University, Espoo, Finland, 24 September 2021.
15. Nagamori, M.; Mackey, P.J.; Tarassoff, P. Copper solubility in FeO-Fe₂O₃-SiO₂-Al₂O₃ slag and distribution equilibria of Pb, Bi, Sb and As between slag and metallic copper. *Met. Trans. B* **1975**, *6*, 295–301. [[CrossRef](#)]

16. Anindya, A. Minor Elements Distribution during the Smelting of WEEE with Copper Scrap. Ph.D. Thesis, RMIT University, New Delhi, India, 2021.
17. Shuva, M.A.H.; Rhamdhani, M.A.; Brooks, G.A.; Masood, S.; Reuter, M.A. Thermodynamics data of valuable elements relevant to e-waste processing through primary and secondary copper production: A review. *J. Clean. Prod.* **2016**, *131*, 795–809. [[CrossRef](#)]
18. Avarmaa, K.; O'Brien, H.; Johto, H.; Taskinen, P. Equilibrium Distribution of Precious Metals Between Slag and Copper Matte at 1250–1350 °C. *J. Sustain. Met.* **2015**, *1*, 216–228. [[CrossRef](#)]
19. Shishin, D.; Hidayat, T.; Chen, J.; Hayes, P.C.; Jak, E. Experimental Investigation and Thermodynamic Modeling of the Distributions of Ag and Au Between Slag, Matte, and Metal in the Cu–Fe–O–S–Si System. *J. Sustain. Metall.* **2019**, *5*, 240–249. [[CrossRef](#)]
20. Klemettinen, L.; Avarmaa, K.; Taskinen, P. Trace Element Distributions in Black Copper Smelting. *World Metall. Erzmetall* **2017**, *70*, 257–264.
21. Sineva, S.; Shevchenko, M.; Shishin, D.; Hidayat, T.; Chen, J.; Hayes, P.C.; Jak, E. Phase Equilibria and Minor Element Distributions in Complex Copper/Slag/Matte Systems. *JOM* **2020**, *72*, 3401–3409. [[CrossRef](#)]
22. Klemettinen, L.; Avarmaa, K.; O'Brien, H.; Taskinen, P.; Jokilaakso, A. Behavior of Tin and Antimony in Secondary Copper Smelting Process. *Minerals* **2019**, *9*, 39. [[CrossRef](#)]
23. Avarmaa, K. Thermodynamic Properties of WEEE-Based Minor Elements in Copper Smelting Processes. Ph.D. Thesis, Aalto University, Espoo, Finland, 20 September 2019.
24. Klemettinen, L.; Avarmaa, K.; Taskinen, P.; Jokilaakso, A. Behavior of nickel as a trace element and time-dependent formation of spinels in WEEE smelting. In Proceedings of the Extraction 2018, Ottawa, Canada, 26–29 August 2018.
25. Shishin, D.; Hidayat, T.; Chen, J.; Hayes, P.C.; Jak, E. Combined experimental and thermodynamic modelling investigation of the distribution of antimony and tin between phases in the Cu–Fe–O–S–Si system. *Calphad* **2019**, *65*, 16–24. [[CrossRef](#)]
26. Takeda, Y. Miscibility Gap in the CaO–SiO₂–Cu₂O–Fe₃O₄ System under Copper Saturation and Distribution of Impurities. *Mater. Trans. JIM* **1993**, *34*, 937–945. [[CrossRef](#)]
27. Johnston, M.D.; Jahanshahi, S.; Zhang, L.; Lincoln, F.J. Effect of Slag Basicity on Phase Equilibria and Selenium and Tellurium Distribution in Magnesia-Saturated Calcium Iron Silicate Slags. *Met. Trans. B* **2010**, *41*, 625–635. [[CrossRef](#)]
28. Dańczak, A.; Klemettinen, L.; O'Brien, H.; Taskinen, P.; Lindberg, D.; Jokilaakso, A. Slag Chemistry and Behavior of Nickel and Tin in Black Copper Smelting with Alumina and Magnesia-Containing Slags. *J. Sustain. Metall.* **2021**, *7*, 1–14. [[CrossRef](#)]
29. Wan, X.; Fellman, J.; Jokilaakso, A.; Klemettinen, L.; Marjakoski, M. Behavior of waste printed circuit board (WPCB) materials in the copper matte smelting process. *Metals* **2018**, *8*, 887. [[CrossRef](#)]
30. Wan, X.; Taskinen, P.; Shi, J.; Klemettinen, L.; Jokilaakso, A. Reaction mechanisms of waste printed circuit board recycling in copper smelting: The impurity elements. *Miner. Eng.* **2021**, *160*, 106709. [[CrossRef](#)]
31. Wan, X.; Kleemola, L.; Klemettinen, L.; Taskinen, P.; Jokilaakso, A. On the kinetic behavior of recycling precious metals (Au, Ag, Pt and Pd) through copper smelting process. *J. Sustain. Metall.* **2021**, *9*, 920–931. [[CrossRef](#)]
32. Klemettinen, L.; Aromaa, R.; Dańczak, A.; O'Brien, H.; Taskinen, P.; Jokilaakso, A. Distribution Kinetics of Rare Earth Elements in Copper Smelting. *Sustainability* **2020**, *12*, 208. [[CrossRef](#)]
33. Davies, R.H.; Dinsdale, A.T.; Gisby, J.A.; Robinson, J.A.J.; Martin, S.M. MTDATA—Thermodynamic and phase equilibrium software from the National Physical Laboratory. *Calphad* **2002**, *26*, 229–271. [[CrossRef](#)]
34. Pouchou, J.L.; Pichoir, F. Basic expression of “PAP” computation for quantitative EPMA. In Proceedings of the 11th International Congress on X-ray Optics and Microanalysis (ICXOM), London, ON, Canada, 4–8 August 1986; Brown, J.D., Packwood, R.H., Eds.; University of Western Ontario: London, ON, Canada, 1986; pp. 249–256.
35. UQAC Pressed Sulfide Pellet Reference Material. Available online: <https://sulfideslasericpms.wordpress.com/rm-available/> (accessed on 9 August 2022).
36. Wilson, S.A.; Ridley, W.I.; Koenig, A.E. Development of sulfide calibration standards for the laser ablation inductively-coupled plasma mass spectrometry technique. *J. Anal. Atom. Spectrom.* **2002**, *17*, 406–409. [[CrossRef](#)]
37. Jochum, K.P.; Weis, U.; Stoll, B.; Kuzmin, D.; Yang, Q.; Raczek, I.; Jacob, D.E.; Stracke, A.; Birbaum, K.; Frick, D.A.; et al. Determination of Reference Values for NIST SRM 610-617 Glasses Following ISO Guidelines. *Geostand. Geoanal. Res.* **2011**, *35*, 397–429. [[CrossRef](#)]
38. van Achterberg, E.; Ryan, C.; Jackson, S.E.; Griffin, W.L. *Data Reduction Software for LA-ICP-MS. Appendix 3 in Laser Ablation ICP-MS in the Earth Sciences: Principles and Applications*; Short Course Series; Mineralogical association of Canada: Quebec City, QC, Canada, 2001; Volume 29, pp. 239–243. ISBN 978-092-12942-9-0.
39. Takeda, Y.; Ishiwata, S.; Yazawa, A. Distribution equilibria of minor elements between liquid copper and calcium ferrite slag. *Trans. Jpn. Inst. Met.* **1983**, *24*, 518–528. [[CrossRef](#)]
40. Yazawa, A.; Takeda, Y. Equilibrium Relations between Liquid Copper and Calcium Ferrite Slag. *Trans. Jpn. Inst. Met.* **1982**, *23*, 328–333.